ROYAL SOCIETY
OF CHEMISTRY

PAPER

Check for updates

The thermodynamic origins of chiral twist in monolayer assemblies of rod-like colloids†

Yawei Liu, [iD] *[a,b] Jared A. Wood, [iD] [a,c] Achille Giacometti [iD] [d,e] and Asaph Widmer-Cooper [iD] *[a,c]

The propagation of chirality across scales is a common but poorly understood phenomenon in soft matter. Here, using computer simulations, we study twisted monolayer assemblies formed by both chiral and achiral rod-like particles in the presence of non-adsorbing polymer and characterise the thermodynamic driving forces responsible for the twisting. We observe assemblies with both like and inverted chirality relative to the rods and show that the preferred twist is already determined during the initial stage of the self-assembly. Depending on the geometry of the constituent rods, the chiral twist is regulated by either the entropy gain of the polymer, or of the rods, or both. This can include important contributions from changes in both the surface area and volume of the monolayer and from rod fluctuations perpendicular to the monolayer. These findings can deepen our understanding of why chirality propagates and of how to control it.

1. Introduction

Colloidal suspensions composed of anisotropic particles can undergo self-assembly that involves the propagation of chirality from the single-particle level to the macroscopic level, and so have emerged as a versatile platform for understanding this common phenomenon in soft matter.[1–5] Cholesteric liquid crystals are a well-known example, but there are many others. This includes the behaviour of colloidal suspensions of DNA, viruses, peptides, polysaccharides and various synthetic nanoparticles.[6–12] While discussion continues about the physi-

[a]ARC Centre of Excellence in Exciton Science, School of Chemistry, University of Sydney, Sydney, New South Wales 2006, Australia. E-mail: ywliu@ipe.ac.cn, asaph.widmer-cooper@sydney.edu.au

[b]Beijing Key Laboratory of Ionic Liquids Clean Process, CAS Key Laboratory of Green Process and Engineering, State Key Laboratory of Multiphase Complex Systems, Institute of Process Engineering, Chinese Academy of Sciences, Beijing, 100190, China

[c]The University of Sydney Nano Institute, University of Sydney, Sydney, New South Wales 2006, Australia

[d]Dipartimento di Scienze Molecolari e Nanosistemi, Università Ca' Foscari di Venezia Campus Scientifico, Edificio Alfa, via Torino 155, 30170 Venezia Mestre, Italy

[e]European Centre for Living Technology (ECLT) Ca' Bottacin, 3911 Dorsoduro Calle Crosera, 30123 Venice, Italy

†Electronic supplementary information (ESI) available: Effect of the number of spheres in one rod; effect of the bin size to determine the excluded volume; free energy changes for monolayers composed of different numbers of rods; brief review of the continuum theory for colloidal membranes; density profiles and volume changes of assembled monolayers; monolayers held together by explicit attraction. See DOI: https://doi.org/10.1039/d2nr05230j

cal levers that can be used to control the phenomenon,[13–19] its potential application in areas including optics, catalysis, and sensing is already being explored,[20–22] and will likely accelerate in light of advances in the synthesis of anisotropic and chiral nanoparticles.[12,23–25] It is therefore important to have a better understanding of the forces which control the propagation of chirality in these systems, and which can even drive changes in surface topology.[26]

One typical such colloidal suspension is a mixture consisting of rod-like particles and non-adsorbing polymers in a good solvent. In these rod–polymer mixtures, the polymers, which behave as random coils with a radius of gyration r_g, can provide an effective attraction between the rods *via depletion forces*,[27] and thus drive the rods to assemble into diverse ordered structures.[28,29] For example, two-dimensional colloidal membranes can form in a suspension of filamentous viruses and dextran.[30] These colloidal membranes are liquid-like monolayer assemblies, and often have a round-shaped edge in which the constituent viruses are twisted and exhibit a chiral distribution of their orientations.[31,32]

This chiral twist is characteristic of these nearly two-dimensional systems and is very different from the more common cholesteric twist observed in bulk (*i.e.*, three dimensional) chiral assembly.[33] The former one is commonly known as "double twist" to distinguish it from the cholesteric (single) twist. The double twist cannot be spatially uniform in the bulk and always occurs with other deformations, with typical examples being twist-bend and splay-twist textures.[34] While the driving mechanism for the cholesteric twist is relatively well understood, it remains elusive for the double twist in

Paper

colloidal membranes and has so far defied a complete explanation, notwithstanding recent attempts. For instance, an entropically-motivated continuum theory has been developed to explain the experimental behaviour of these colloidal membranes.[35] Briefly, the entropy, manifested through the viruses as Frank elastic energy for the twist distortion and through the polymers as an effective surface tension for the excluded volume, drives the chiral twist of the membranes. This description further assumes that the membranes are incompressible in the continuum limit.

To test the generality of this theory, and to serve as an important complementary tool to interpret experimental results, it would be useful to study such membranes using a particle-based simulation approach. This would be especially useful for analyzing small clusters formed at the onset of the self-assembly process where continuum descriptions often break down. To our knowledge, however, existing simulation studies of twisted membranes have been limited to the case of achiral rods which lack intrinsic chirality.[31] In this work, we therefore study membranes formed by both achiral rods and chiral rod-like helices[36] using Langevin dynamics (LD) simulations and characterise the thermodynamic driving forces responsible for the propagation of chirality in these systems.

2. Model and method

2.1. Models for rod–polymer suspensions

The rod–polymer suspensions were described using a continuous potential model that approximates the well-known Asakura-Oosawa-Vrij (AO) model:[27,37] (achiral) straight rods, described as *hard spherocylinders*, were represented by a rigid linear chain of length L consisting of overlapping hard spheres of diameter D (Fig. 1a); chiral rods, described as *hard helices*,
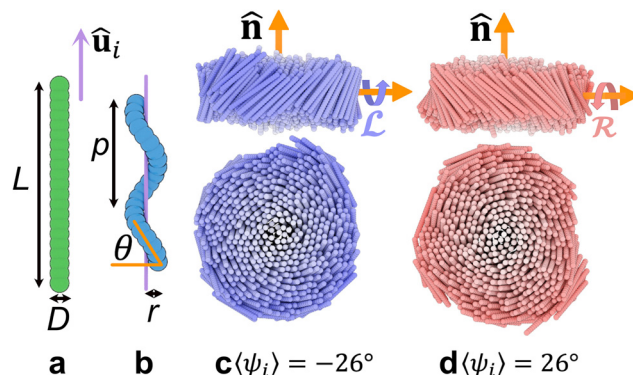

Fig. 1 Spontaneous twist in monolayers of rods. (a) An achiral straight rod of length L and diameter D. (b) A chiral rod (left-handed helix) with contour length L, diameter D, pitch p and radius r. θ quantifies the inclination angle of the rod.[47] (c and d) Side-view and top-view of (c) left-handed ($\mathcal{L}$) and (d) right-handed ($\mathcal{R}$) monolayers composed of straight rods, with the color indicating the normalised tilted angle ($\psi_i/|\psi_i^{\mathrm{max}}|$) between the rod axis $\hat{\mathbf{u}}_i$ and the nematic director $\hat{\mathbf{n}}$.

were modeled as a set of hard spheres having diameter D evenly arranged along a helical line of contour length L, pitch p and radius r (Fig. 1b); and the non-adsorbing polymers were modelled as spheres with diameter $d = 2r_g$ that are freely interpenetrable to each other but experience a hard repulsion from the rod spheres. For simplicity, we set the diameter of polymer spheres $d = D$. In our simulations, the hard-core potential between rod–rod (rr) and between rod–polymer (rp) sphere pairs was replaced by a continuous pseudo-hard-core potential, *i.e.*, $U^{\alpha\beta}(r) = 50(50/49)^{49}\varepsilon[(\sigma/r)^{50} - (\sigma/r)^{49}]$ ($\alpha\beta\in$rr,rp) truncated and shifted at $r_{\mathrm{cut}}^{\alpha\beta} = (50/49)\sigma$, where r is the centre-to-centre distance between the spheres, ε is the energy parameter, and σ is the distance parameter with $\sigma = D$. Besides, for all rods used in this work, the distance between consecutive spheres is $0.5D$, which is sufficient to remove side effects associated with surface roughness (ESI S1†).

While an implicit polymer model for (achiral) straight rods such as that in refs. 38–40 can allow us to simulate large systems, the corresponding model for helical rods is lacking and developing an accurate implicit polymer model for hard helices, especially in the case of large polymers, could be quite challenging.[41]

2.2. Langevin dynamics simulation details

All LD simulations were carried out using LAMMPS[42] at a dimensionless temperature $k_{\mathrm{B}}T/\varepsilon = 1$ (where k_{B} is the Boltzmann constant and T is the temperature). In the simulations, rod and polymer spheres are subjected to three forces: the conservative force f^{C} computed via the pairwise interactions (*i.e.*, the pseudo-hard-core potential); the friction force $f^{\mathrm{F}} = -(m/\gamma)v$ with m the mass, γ the damping factor, and v the velocity of the sphere; and the random force $f^{\mathrm{R}} \propto \sqrt{k_{\mathrm{B}}Tm/(\Delta t\gamma)}$ with Δt the time step. All simulations were performed in a box with periodic boundary conditions. The velocity-Verlet algorithm was used to integrate the equations of

Dr Yawei Liu is an Associate Professor at the Institute of Process Engineering of Chinese Academy of Sciences. Prior to this he was a Postdoctoral Researcher at the University of Sydney during 2017–2021, a visiting PhD student at the University of Cambridge during 2014–2016. He received his PhD degree in Chemical Engineering from Beijing University of Chemical Technology in 2017.

Yawei Liu

His research is focused on developing and applying multiscale analytical and computational methods, mainly molecular simulations, to study soft matters, with a particular interest in how the nanoscale interfacial structures influence and regulate the behaviors of fluids and particles in the system. His current research topics include nanobubbles, nanofluidics and assembly of nanomaterials.

motion with a time step $\Delta t = 0.001\tau$ where $\tau = D\sqrt{m/(k_B T)}$, and the damping factor was set to be $\gamma = 1\tau$. In all simulations, we set the masses of one polymer and one rod $m_p = m_r = m = 1$. Simulations of large monolayers were performed in an isothermal-isobaric (NPT) ensemble. A Berendsen barostat with a time constant of 1τ was applied. Most simulations were initialised with $N_r = 480$ rods in a single hexagonally packed layer surrounded by $N_p = 40\,000$ polymer spheres in a box with initial dimensions $44 \times 44 \times 21D^3$. Initial configurations with different chiral twists were also used to confirm that only one handedness was stable. At least 10 independent simulations with different initial configurations were performed for each rod shape, and all simulations were run for at least 5×10^6 steps to collect enough configurations at the equilibrium state.

2.3. Free energy calculations

Simulations used for measuring changes in the free energy ($\Delta\Omega_{\text{total}}$) as a function of the twist ($\langle\psi_i\rangle$, see its definition in next section) were performed in a semi-grand canonical ($\mu_p VT$) ensemble with $N_r = 2$–61 rods. During the simulations, 1000 GCMC insertion and deletion moves were performed every 1000 LD steps to maintain the chemical potential of the polymers (μ_p). Simulations were initialised with N_r rods in a single hexagonally packed layer surrounded by ~2000 polymer spheres in a box with dimensions $15 \times 15 \times 15D^3$. The values of $\Delta\Omega_{\text{total}}$ as a function of $\langle\psi_i\rangle$ were evaluated by means of the umbrella sampling (US) method.[43] We imposed a harmonic spring biasing potential given by $U = 0.5k[\langle\psi_i\rangle - \langle\psi_i\rangle_0]^2$ on the system using the Colvars package.[44] Here, k is the spring constant, $\langle\psi_i\rangle_0$ is the desired twist, and $\langle\psi_i\rangle$ is the actual twist in the monolayer. Under the biasing potential, the monolayer is forced to stay in a pseudo-equilibrium state with $\langle\psi_i\rangle$ fluctuating around $\langle\psi_i\rangle_0$. Different twisted states can be described by a series of values with $\langle\psi_i\rangle_0 \in (\langle\psi_i\rangle_{\min}, \langle\psi_i\rangle_{\max})$. In our simulations, $k = 1k_B T/\text{deg}^2$, $\langle\psi_i\rangle_{\min} = -24°$, $\langle\psi_i\rangle_{\max} = 24°$, and the increment of $\langle\psi_i\rangle_0$ was 1° or 2°. For each given $\langle\psi_i\rangle_0$, the system was equilibrated for 2×10^6 steps followed by another 2×10^6 steps production run in which data was accumulated every 1000 LD steps. Finally, the WHAM algorithm[45] was used to calculate the free energy change $\Delta\Omega_{\text{total}}$ as a function of $\langle\psi_i\rangle$. For each monolayer, 10 independent simulations were carried out to obtain good statistics. Meanwhile, to prevent the disassembly of small monolayers, additional spring forces were imposed on the rod to move it back when the distance from the centre of the rod to the centre of the monolayer is larger than a critical value r_c, where $r_c = 0.75D$ for $N_r = 2$, $r_c = 1.5D$ for $N_r = 7$, $r_c = 3.0D$ for $N_r = 19$, $r_c = 4.5D$ for $N_r = 37$ and $r_c = 6.0D$ for $N_r = 61$. These critical values are larger than the equilibrium radii of the respective stable monolayers.

2.4. Excluded volume calculations

During the production stage of US simulations, we sampled configurations every 5000 steps and computed the excluded volume (*i.e.*, ΔV_{exc}) for polymer spheres due to rods and the corresponding contributions from the volume and the surface area of the monolayer (*i.e.*, $\Delta V_{\text{exc}}^{\text{bulk}}$ and $\Delta V_{\text{exc}}^{\text{surf}}$). For a given con-figuration, all rod spheres that had at least one polymer neighbour within $1.5D$ from their centre were classified as surface rod–spheres, and the rest were classified as bulk rod–spheres. To compute the excluded volumes, the whole system was divided into many small cubic bins with an edge length of $l = 0.5D$. We confirmed that using a smaller value of l (*e.g.*, $l = 0.25D$, ESI S2†) gave similar results. A bin was occupied by rods if there was at least one rod–sphere whose centre was less than $1.0D$ (corresponding to the polymer diameter) from the bin's centre, and the volume of the bin contributed to $\Delta V_{\text{exc}}^{\text{surf}}$ if all rod–spheres occupying this bin were surface rod–spheres, otherwise it contributed to $\Delta V_{\text{exc}}^{\text{bulk}}$. The final value of the excluded volume at a given $\langle\psi_i\rangle$ was averaged over all configurations collected at the corresponding $\langle\psi_i\rangle_0$. For these calculations, the Freud Python package[46] was used to analyse the simulation data.

2.5. Suppressing perpendicular fluctuations

In the simulations for monolayers without rod fluctuations perpendicular to the monolayer, the centres of mass of all rods were constrained on a common plane *via* harmonic spring forces using a spring constant of $1000k_B T/D^2$.

3. Results and discussion

3.1. Spontaneous twist in monolayers

We first considered monolayers composed of (achiral) straight rods with length of $L = 10D$ (Fig. 1a). Fig. 1c and d show equilibrium configurations obtained from simulations with $N_r = 480$ rods surrounded by $N_p = 40\,000$ polymer spheres at the pressure $P = 1.2k_B T/D^3$. The rods are parallel to the normal axis (*i.e.*, the nematic director $\hat{\mathbf{n}}$) at the centre, but tilt with increasing magnitude around the radial axis away from the centre. In multiple independent simulations started with an untwisted configuration, the monolayer shows nearly equal probability to end up showing left-handed ($\mathcal{L}$) or right-handed ($\mathcal{R}$) twist. Such monolayers, with roughly square edge profiles, are also predicted by the continuum theory and have been observed in experiments for small colloidal membranes.[35]

To evaluate the degree of twist in the monolayers, we used the average tilt angle of rods with respect to the nematic director, defined as

$$\langle\psi_i\rangle = \left\langle \frac{\hat{\mathbf{r}}_i \cdot (\hat{\mathbf{n}} \times \hat{\mathbf{u}}_i)}{|\hat{\mathbf{r}}_i \cdot (\hat{\mathbf{n}} \times \hat{\mathbf{u}}_i)|} \cos^{-1}(|\hat{\mathbf{n}} \cdot \hat{\mathbf{u}}_i|) \right\rangle, \quad (1)$$

where $\hat{\mathbf{r}}_i$ is unit vector connecting the center-of-mass of the monolayer and the center-of-mass of rod i, $\hat{\mathbf{u}}_i$ is the a unit vector along the long axis of the rod and $\langle...\rangle$ indicates an average over all rods in the monolayer and all configurations collected at the equilibrium state. $\langle\psi_i\rangle$ is negative for the $\mathcal{L}$ twist and positive for the $\mathcal{R}$ twist (Fig. 1c and d).

3.2. Phase diagram of chirality in monolayers

We then studied monolayers of left-handed hard helices with $L = 10$ and varying r and p (Fig. 1b). A summary of the results
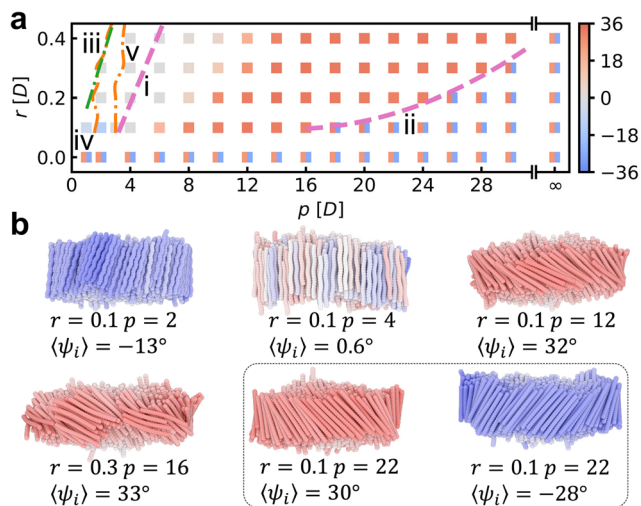
Fig. 2 Phase diagram of chirality in monolayers. (a) The phase diagram shows the chirality of monolayer assemblies of hard rods with $L = 10$ and varying r and p at $P = 1.2$. All symbols are colored according to $\langle \psi_i \rangle$ [eqn (1)] of the corresponding monolayer. The handedness of the monolayer with respect to that of the constituent hard rods can be the same (blue square), opposite (red square), or mixed with either $\mathcal{R}$ or $\mathcal{L}$ (bi-colored square). Note that all symbols with $r = 0$ or $p = \infty$ represent the case of straight rods. Lines (i) and (ii) indicate the approximate phase boundaries for monolayers. Lines (iii–v), provided for comparison, indicate the phase boundaries between the same and opposite regions for bulk cholesteric phases. Line (iii) is given by the critical inclination angle $\theta = 45°$,[2,39] while Lines (iv–v) were obtained using density functional theory at (iv) low and (v) high volume fractions, respectively.[48] (b) Typical snapshots of stable monolayers obtained from simulations using different left-handed helices.

obtained from simulations with $N_r = 480$ at $P = 1.2 k_B T/D^3$ is reported in Fig. 2. In the phase diagram (Fig. 2a), we can identify the values of r and p that give rise to a chiral twist, whose handedness with respect to that of the constituent rods is (i) the same (*e.g.*, $r = 0.1$, $p = 2$), (ii) the opposite (*e.g.*, $r = 0.1$, $p = 12$), or (iii) mixed with either $\mathcal{R}$ or $\mathcal{L}$ (*e.g.*, $r = 0.1$, $p = 22$) (Fig. 2b).

In Fig. 2a, Line (v) is the phase boundary between same and opposite regimes for the corresponding cholesteric phases at high volume fractions obtained using density functional theory.[48] We can see that, in comparison, the corresponding phase boundary for monolayers [*i.e.*, Line (i)] is shifted toward larger values of p at $r > 0.1$. Such shifting is also observed in cholesteric phases when the packing density of helices increases [compare Lines (iii)/(iv) to Line (v) in Fig. 2a]. Thus the difference between Line (i) and Line (v) is likely due to the higher rod packing fraction in the monolayers (0.6–0.7) compared to in the bulk cholesteric phases (0.35–0.5).[48]

For most helices, however, their monolayer assemblies and cholesteric phases have the same handedness, supporting the experimental observation of consistent chirality between the two for rod-shaped viruses.[32] For weakly curled helices in the mixed regime, the monolayers can be either $\mathcal{R}$ or $\mathcal{L}$, while the cholesteric phases may only exhibit weak opposite handed-

ness.[48] As will be elaborated later, the driving mechanism of this chiral monolayer assembly is very different from the bulk cholesteric chiral assembly that was originally predicted by Straley[33] and recently confirmed by density functional theory[47,48] and numerical simulations.[49]

From the phase diagram, we also can see that the degree of twist (*i.e.*, $\langle \psi_i \rangle$) is a non-monotonic function of the intrinsic pitch of the rods (*i.e.*, p), which is consistent with the behaviour of bulk cholesteric phases formed by hard helices.[47,49] Starting at $p = \infty$ (*i.e.*, straight rods), the magnitude of $\langle \psi_i \rangle$ increases as p decreases, and reaches a maximum for moderately curled helices (*e.g.*, $r = 0.1$, $p = 12$ and $r = 0.3$, $p = 16$) in the opposite regime, before decreasing to 0 for helices at the phase boundary between same and opposite regimes (*e.g.*, $r = 0.1$, $p = 4$) (Fig. 2b). In the same regime, $|\langle \psi_i \rangle|$ is small, but our results at $r = 0.1$ show that here again $|\langle \psi_i \rangle|$ first increases and then deceases as p decreases (Fig. 2a).

3.3. Thermodynamic origins of chiral twist

To study the thermodynamic origins of chiral twist in these monolayer assemblies, we considered a monolayer of N_r rods in a sea of polymer spheres at fixed volume V and temperature T. This system was kept in osmotic equilibrium with a large reservoir containing the pure polymer solution at fixed fugacity $z_p = \exp(\mu_p/k_B T)$ where μ_p is the polymer chemical potential. The grand potential of the system can be written as $\Omega_{total}(N_r, V, T, \mu_p) = F_r - z_p(V - V_{exc})k_B T$, where F_r is the Helmholtz energy of the rods and V_{exc} is the volume excluded to the polymers by the hard rods.[28,50] The second term on the right is the free energy of the polymers Ω_p. V_{exc} can be further divided into a bulk term and a surface term associated to the volume and surface area of the monolayer, respectively. Thus, we obtain the change in free energy expressed as

$$
\begin{aligned}
\Delta\Omega_{total} &= \Delta F_r + \Delta\Omega_p \\
&= \Delta F_r + z_p k_B T \Delta V_{exc} \\
&= \Delta F_r + z_p k_B T \left(\Delta V_{exc}^{bulk} + \Delta V_{exc}^{surf} \right).
\end{aligned} \tag{2}
$$

Both ΔF_r and ΔV_{exc} depend on the twisting state of rods in the monolayer. We measured $\Delta\Omega_{total}$ as a function of $\langle \psi_i \rangle$ in a semi-grand canonical ($\mu_p VT$) ensemble with fixed N_r at $z_p = 1.2$ (corresponding to $P = 1.2 k_B T/D^3$ in the previous simulations). The twist was constrained using the US approach, while ΔV_{exc}^{bulk} and ΔV_{exc}^{surf} were numerically calculated.

We performed a series of US simulations to calculate the changes in free energy as a function of the twist for monolayers formed by $N_r = 2$–61 rods with varying p (ESI S3†). The average twist of stable monolayers monotonically increases as the monolayer size increases, which is qualitatively consistent with the theoretical description for small colloidal membranes in which the tile angles of rods at the edge have yet to reach the limiting value of 90°.[35] More importantly, we found that simulating tens of rods is sufficient to capture the chiral behaviour exhibited by the large monolayers shown in Fig. 2, indicating that the chirality of these monolayers is determined already during the onset of the self-assembly process.
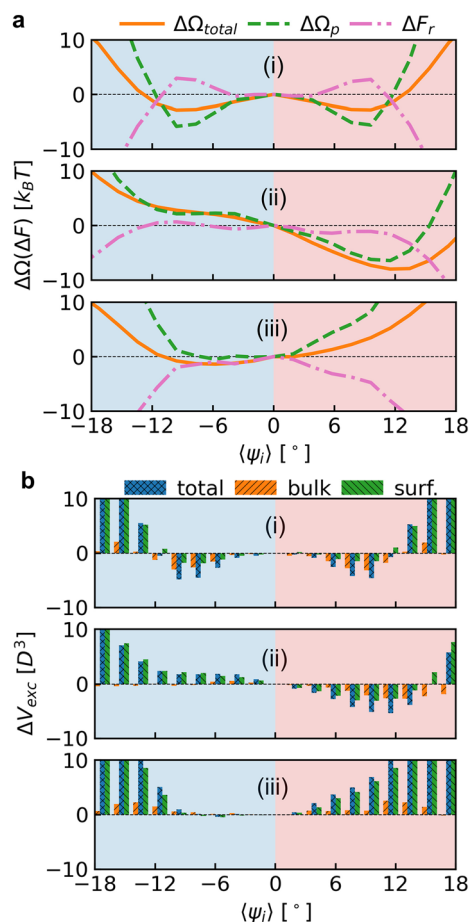
Fig. 3 The thermodynamic origins of chiral twist in monolayers of different rods. (a) The changes in free energy ($\Delta\Omega_{\text{total}}$, ΔF_r and $\Delta\Omega_p$) as a function of the twist ($\langle\psi_i\rangle$) for monolayers formed by $N_r = 37$ (i) straight rods ($r = 0.0$, $p = \infty$), (ii) left-handed moderately curled helices ($r = 0.1$, $p = 12$), and (iii) left-handed highly curled helices ($r = 0.1$, $p = 2$). (b) The corresponding changes of excluded volume (ΔV_{exc}, $\Delta V_{\text{exc}}^{\text{bulk}}$ and $\Delta V_{\text{exc}}^{\text{surf}}$).

Fig. 3a shows $\Delta\Omega_{\text{total}}$ *vs.* $\langle\psi_i\rangle$ for three typical monolayers made up of 37 straight rods or left-handed helices. For the monolayer of straight rods (*i.e.*, $r = 0$), the two identical minima at $\langle\psi_i\rangle > 0$ and $\langle\psi_i\rangle < 0$ in the curve of $\Delta\Omega_{\text{total}}$ indicate the stable twist is equally likely to be $\mathcal{R}$ or $\mathcal{L}$. For the monolayer of helices, only one local minimum appears in the curve of $\Delta\Omega_{\text{total}}$ and is located at $\langle\psi_i\rangle > 0$ for the left-handed moderately curled helices (*i.e.*, $r = 0.1$, $p = 12$) and at $\langle\psi_i\rangle < 0$ for the left-handed highly curled helices (*i.e.*, $r = 0.1$, $p = 2$), consistent with the behaviour of the larger monolayers summarised in Fig. 2a.

The decomposition of $\Delta\Omega_{\text{total}}$ in eqn (2) reveals that chiral twist in these monolayers is stabilised by different driving forces depending on the rod shape. As shown in Fig. 3a(i), the twist in monolayers of straight rods is driven by the entropy gain of the polymers with respect to the untwisted state (*i.e.*, the decease in $\Delta\Omega_p$), but further twisting beyond the equilibrium state is also prevented by the rapidly increasing entropy loss of the polymers at larger $|\langle\psi_i\rangle|$. The rod entropy in this

case shows an almost opposite dependence on $\langle\psi_i\rangle$, but the polymer entropy dominates and stabilises the twist in the monolayer. For the monolayer of moderately curled helices [Fig. 3a(ii)], the polymer entropy also dominates and leads to a single stable twist, but now entropy gain from the rods also contributes. In sharp contrast, for the monolayer of highly curled helices [Fig. 3a(iii)], the single stable twist is entirely driven by the rod entropy, competing against the entropy loss of the polymers.

The polymer entropy is related to changes in the volume excluded to polymers (ΔV_{exc}), which is determined by both the volume and the surface area of the monolayer. Fig. 3b shows the change in ΔV_{exc} and its volume/surface components when twisting the three monolayers discussed in the previous paragraph. This reveals that not only the surface area but also the volume of the monolayers changes significantly during the twisting process. Especially for monolayers of straight rods [Fig. 3b(i)], the decrease in the volume acts as the major driving force for twisting.

3.4. Comparison with continuum theory

Having shown that different entropy components can drive rod monolayers to twist, we now compare our results with the continuum theory developed to describe such colloidal membranes.[35] The continuum theory is based on a relatively simple physical picture (ESI S4†): that the twist is driven mainly by the entropy gained by the polymers when the membrane surface area is minimised at constant membrane volume. In this model, the polymer entropy is invariant under chirality inversion and does not contribute to the preference of the handedness, regardless of the chirality of the rods. The preferred handedness is instead attributed to an entropy term in the Frank elastic energy of the rods, whose magnitude depends on the preferred twist wavenumber that implicitly contains the chiral features of the rods.

In contrast, our simulation results reveal the existence of more complex thermodynamic behaviour. First, while the polymer entropy often drives twisting, it can also oppose twisting, with the rod entropy instead driving twisting in those cases [*e.g.*, Fig. 3a(iii)]. Second, the polymer entropy is asymmetric under chirality inversion for monolayers of helical particles and contributes to the preference of the handedness in these cases [*e.g.*, Fig. 3a(ii)]. This indicates that, at best, the Frank elastic energy in the continuum theory can depend on polymer concentration. Third, the constant-volume assumption in the continuum theory clearly breaks down, at least for the small assemblies considered here, indicating that the variation of the polymer entropy involves contributions from not only the surface area but also the volume of the monolayer (Fig. 3b).

Recent theoretical and experimental work[51–53] has also concluded that the volume change upon twist plays a crucial role in determining the geometry and stability of colloidal membranes of rod-like particles. The geometric frustration between double-twist and splay causes the twisted monolayer to have a hyperbolic edge (*i.e.*, "splay-twist" texture[51]), and the splay of

rods away from the monolayer midplane leads to a local volume expansion, which is most significant at the top and the bottom of the monolayer edge. Based on this geometric argument, using a combination of experiments and theory in which the variation of rod density is considered, Miller *et al.*[53] demonstrated that for the colloidal rafts in the membranes composed of rigid rods of different lengths, the splay deformation causes expansion and compression of the inner and outer raft edges, respectively, and their competition results in spontaneous twist even for achiral systems and non-monotonic dependence of the stable twist as a function of the raft size. As for our simulated monolayers which are assembled from monodisperse rods in non-adsorbing polymers, the diffuse interfacial region exhibits a clear decline of the rod density away from the midplane, especially at the edges [Fig. S5(a)†], but we did not observe an obvious hyperboloid-like shape. Only when the perpendicular fluctuations of the rods are suppressed and their centers are confined at the 2D midplane (which is the same as the theoretical model in ref. 53), does our monolayer exhibit a hyperboloid-like shape [Fig. S5(b)†]. Moreover, in our systems, the total volumes of small monolayers (which are made up of 37 rods in our US simulations) are always decreasing during the initial twisting process (Fig. S6†), suggesting that the volume expansion due to the splay deformation does not dominate, at least in these small monolayers. All these results suggest that the volume change due to twist is important to the stable texture in various colloidal membranes of rod-like particles and thus should not be ignored in theoretical models.

3.5. The role of perpendicular fluctuations

Finally, we considered a special entropy contribution from rods related to their fluctuations perpendicular to the monolayer. Fig. 4c shows $\Delta\Omega_{\text{total}}$ *vs.* $\langle\psi_i\rangle$ for the three example monolayers when the centres-of-mass of all rods are constrained to the midplane of the monolayer. The rod fluctuations out of the plane are expected to produce surface roughness and so increase the volume excluded to the polymers. We found that suppressing the fluctuations resulted in more entropy gain for the polymers upon twisting for monolayers of straight rods and moderately curled helices [see larger changes of $\Delta\Omega_{\text{p}}$ in Fig. 4a(i) and (ii) compared to that in Fig. 3a(i) and(ii)]. This stabilises the twisted states for these monolayers, and even adds a new metastable twisted state for the monolayer of moderately curled helices [Fig. 4a(ii)]. In contrast, for the monolayer of highly curled helices, the polymer entropy increases dramatically upon twisting when the fluctuations are suppressed, causing the original weakly-stable twisted state to disappear [Fig. 4a(iii)]. These results are consistent with unconstrained simulations of large monolayers (Fig. 4b), and clearly show that rod fluctuations perpendicular to the monolayer have important effects on the stability of the chiral twists that depend on the shape of the individual rods.

We note that such contributions from rod fluctuations perpendicular to the monolayer are either ignored in continuum models of colloidal membranes or only taken into account in a
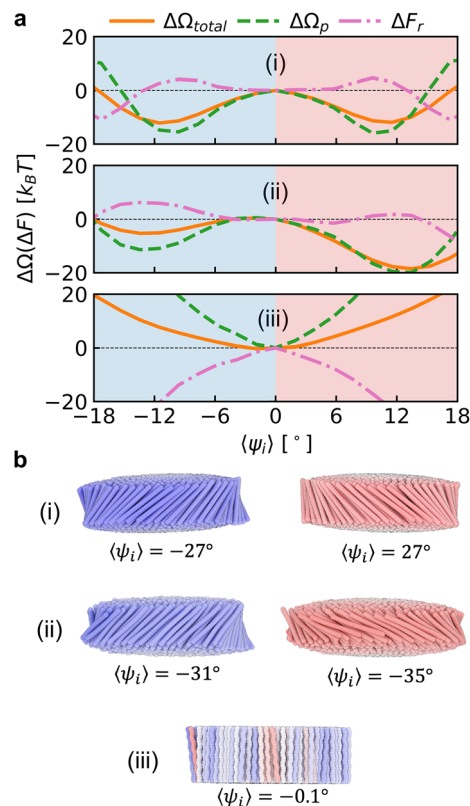

Fig. 4 The role of perpendicular fluctuations. (a) The changes in free energy ($\Delta\Omega_{\text{total}}$, ΔF_r and $\Delta\Omega_{\text{p}}$) as a function of the twist ($\langle\psi_i\rangle$) for monolayers formed by $N_r = 37$ (i) straight rods ($r = 0.0$, $p = \infty$), (ii) left-handed moderately curled helices ($r = 0.1$, $p = 12$), and (iii) left-handed highly curled helices ($r = 0.1$, $p = 2$) when the fluctuations perpendicular to the plane of the monolayer are artificially suppressed. (b) Typical snapshots of large equilibrated monolayers formed by $N_r = 480$ rods (corresponding to those in a), obtained from simulations without rod fluctuations perpendicular to the monolayer.

simplistic manner (which is not curliness-dependent)[35] (ESI S4†). Our simulation results, however, indicate that these fluctuations can play a crucial role in the stability of the chiral twist, and thus may need to be accurately described in order to predict the stable chiral twist.

4. Conclusions

In summary, we have used a simple model to characterise spontaneous chiral twist in monolayers assembled from either achiral or chiral rods in non-adsorbing polymer solutions, and thus to reveal the thermodynamic driving forces responsible for chirality propagation from single particles to their assemblies. Note that the chiral twist discussed in this work is the double twist, which is distinct from the cholesteric (single) twist.[34]

Depending on the geometry of the constituent rods, their monolayer assemblies exhibit a broad range of chiral behaviour, including variations in handedness and twist magnitude.

Compared to the constituent rods, the (achiral) straight rods and weakly curled helices form monolayers with either $\mathcal{R}$ or $\mathcal{L}$ twist (*i.e.*, the mixed regime), moderately curled helices form monolayers with the opposite handedness (*i.e.*, the opposite regime), and highly curled helices form monolayers with the same handedness (*i.e.*, the same regime). Moreover, the degree of twist in the monolayers is a non-monotonic function of the intrinsic pitch of the helices, with the most twisted monolayers forming from moderately curled helices [Fig. 2(a)].

The thermodynamic forces responsible for spontaneous chiral twist also vary dramatically between different particle shapes. In the mixed and the opposite regimes, the twist in monolayers is mainly driven by the polymer entropy [Fig. 3a (i)]. As the rods becomes more curled, the rod entropy also contributes to the twist, and only the twisted state with the opposite handedness remains stable [Fig. 3a(ii)]. For even more curled helices, only one weakly twisted state with the same handedness is stable, and is entirely driven by the rod entropy [Fig. 3a(iii)].

Our simulation results also indicate important contributions from the volume change upon twist and the rod fluctuations perpendicular to the monolayer that have so far been ignored in continuum theories. Our preliminary results, obtained from Monte Carlo (MC) simulations, for rods held together by explicit attraction rather than polymer depletion indicate a similar complexity (ESI S6†). Overall, we find increasing deviations from current continuum theory as the attractive forces holding the rods together become weaker, regardless of whether they are due to direct energetic or indirect entropic effects (ESI S6†). All these results contribute to our understanding of chirality transmission across scales when chiral objects assemble into larger aggregates.

While our simulations were based on a simplified model for rod-like colloids (*i.e.*, hard spherocylinders and helices), they clearly show that twisted colloidal membranes can also be formed by helical rods, which could be an interesting behaviour to investigate in future experiments by using similar natural and synthetic particles.[1,54–56] Our current work also offers a helpful reference for understanding the behaviour in more complex systems. It would be very useful to consider models which are closer to the chiral rods (*e.g.* fd-virus and DNA origami rods) used in experiments of colloidal membranes. For example, using a "straight and helically-decorated" model[2,57] would allow us to compare the computational and experimental results more directly. Meanwhile, recent experiments have shown that the shape fluctuation of chiral rods also dramatically affects their assembled structures,[58] thus it would be interesting to consider the flexibility of rod-like particles in future work.

Author contributions

Yawei Liu: conceptualization, methodology, investigation, formal analysis, visualization, writing – original draft. Jared A. Wood: conceptualization, methodology, investigation, formal analysis, writing – original draft. Achille Giacometti: funding acquisition, writing – review & editing. Asaph Widmer-Cooper: conceptualization, supervision, resources, funding acquisition, writing – review & editing.

Conflicts of interest

There are no conflicts to declare.

Acknowledgements

References

1 E. Barry, Z. Hensel, Z. Dogic, M. Shribak and R. Oldenbourg, *Phys. Rev. Lett.*, 2006, **96**, 018305.

2 F. Tombolato, A. Ferrarini and E. Grelet, *Phys. Rev. Lett.*, 2006, **96**, 258302.

3 C. Greco and A. Ferrarini, *Phys. Rev. Lett.*, 2015, **115**, 147801.

4 S. Dussi and M. Dijkstra, *Nat. Commun.*, 2016, **7**, 11175.

5 A. Sharma, J. P. Wojciechowski, Y. Liu, T. Pelras, C. M. Wallace, M. Müllner, A. Widmer-Cooper, P. Thordarson and G. Lakhwani, *Cell Rep. Phys. Sci.*, 2020, **1**, 100148.

6 M. Siavashpouri, C. H. Wachauf, M. J. Zakhary, F. Praetorius, H. Dietz and Z. Dogic, *Nat. Mater.*, 2017, **16**, 849–856.

7 J. M. Miller, C. Joshi, P. Sharma, A. Baskaran, A. Baskaran, G. M. Grason, M. F. Hagan and Z. Dogic, *Proc. Natl. Acad. Sci. U. S. A.*, 2019, **116**, 15792–15801.

8 G. Nyström, M. Arcari and R. Mezzenga, *Nat. Nanotechnol.*, 2018, **13**, 330–336.

9 G. Nyström, M. Arcari, J. Adamcik, I. Usov and R. Mezzenga, *ACS Nano*, 2018, **12**, 5141–5148.

10 A. Aggeli, I. A. Nyrkova, M. Bell, R. Harding, L. Carrick, T. C. B. McLeish, A. N. Semenov and N. Boden, *Proc. Natl. Acad. Sci. U. S. A.*, 2001, **98**, 11857–11862.

11 J. Lv, X. Gao, B. Han, Y. Zhu, K. Hou and Z. Tang, *Nat. Rev. Chem.*, 2022, **6**, 125–145.

12 C. Fernández-Rico, M. Chiappini, T. Yanagishima, H. de Sousa, D. G. A. L. Aarts, M. Dijkstra and R. P. A. Dullens, *Science*, 2020, **369**, 950–955.

13 A. B. Harris, R. D. Kamien and T. C. Lubensky, *Rev. Mod. Phys.*, 1999, **71**, 1745–1757.

14 V. Sharma, M. Crne, J. O. Park and M. Srinivasarao, *Science*, 2009, **325**, 449–451.

15 S. M. Morrow, A. J. Bissette and S. P. Fletcher, *Nat. Nanotechnol.*, 2017, **12**, 410–419.

16 P.-P. Wang, S.-J. Yu, A. O. Govorov and M. Ouyang, *Nat. Commun.*, 2017, **8**, 14312.

17 J. Yeom, B. Yeom, H. Chan, K. W. Smith, S. Dominguez-Medina, J. H. Bahng, G. Zhao, W. S. Chang, S. J. Chang, A. Chuvilin, D. Melnikau, A. L. Rogach, P. Zhang, S. Link, P. Král and N. A. Kotov, *Nat. Mater.*, 2015, **14**, 66–72.

18 J. Sun, Y. Li, F. Yan, C. Liu, Y. Sang, F. Tian, Q. Feng, P. Duan, L. Zhang, X. Shi, B. Ding and M. Liu, *Nat. Commun.*, 2018, **9**, 2599.

19 M. Chiappini, T. Drwenski, R. van Roij and M. Dijkstra, *Phys. Rev. Lett.*, 2019, **123**, 068001.

20 M. Hentschel, M. Schäferling, X. Duan, H. Giessen and N. Liu, *Sci. Adv.*, 2017, **3**, 1–13.

21 S. Li, J. Liu, N. S. Ramesar, H. Heinz, L. Xu, C. Xu and N. A. Kotov, *Nat. Commun.*, 2019, **10**, 4826.

22 C. Hao, L. Xu, H. Kuang and C. Xu, *Adv. Mater.*, 2020, **32**, 1–21.

23 S. C. Glotzer and M. J. Solomon, *Nat. Mater.*, 2007, **6**, 557–562.

24 H. E. Lee, H. Y. Ahn, J. Mun, Y. Y. Lee, M. Kim, N. H. Cho, K. Chang, W. S. Kim, J. Rho and K. T. Nam, *Nature*, 2018, **556**, 360–364.

25 G. González-Rubio, J. Mosquera, V. Kumar, A. Pedrazo-Tardajos, P. Llombart, D. M. Solís, I. Lobato, E. G. Noya, A. Guerrero-Martínez, J. M. Taboada, F. Obelleiro, L. G. MacDowell, S. Bals and L. M. Liz-Marzán, *Science*, 2020, **368**, 1472–1477.

26 A. Khanra, L. L. Jia, N. P. Mitchell, A. Balchunas, R. A. Pelcovits, T. R. Powers, Z. Dogic and P. Sharma, *Proc. Natl. Acad. Sci. U. S. A.*, 2022, **119**, e2204453119.

27 S. Asakura and F. Oosawa, *J. Chem. Phys.*, 1954, **22**, 1255–1256.

28 H. N. W. Lekkerkerker and A. Stroobants, *Nuovo Cim. D*, 1994, **16**, 949–962.

29 M. Siavashpouri, P. Sharma, J. Fung, M. F. Hagan and Z. Dogic, *Soft Matter*, 2019, **15**, 7033–7042.

30 E. Barry and Z. Dogic, *Proc. Natl. Acad. Sci. U. S. A.*, 2010, **107**, 10348–10353.

31 T. Gibaud, E. Barry, M. J. Zakhary, M. Henglin, A. Ward, Y. Yang, C. Berciu, R. Oldenbourg, M. F. Hagan, D. Nicastro, R. B. Meyer and Z. Dogic, *Nature*, 2012, **481**, 348–351.

32 T. Gibaud, C. N. Kaplan, P. Sharma, M. J. Zakhary, A. Ward, R. Oldenbourg, R. B. Meyer, R. D. Kamien, T. R. Powers and Z. Dogic, *Proc. Natl. Acad. Sci. U. S. A.*, 2017, **114**, E3376–E3384.

33 J. P. Straley, *Phys. Rev. A*, 1976, **14**, 1835–1841.

34 J. V. Selinger, *Liq. Cryst. Rev.*, 2018, **6**, 129–142.

35 L. Kang, T. Gibaud, Z. Dogic and T. C. Lubensky, *Soft Matter*, 2016, **12**, 386–401.

36 E. Frezza, A. Ferrarini, H. B. Kolli, A. Giacometti and G. Cinacchi, *J. Chem. Phys.*, 2013, **138**, 164906.

37 Y. Liu and A. Widmer-Cooper, *J. Chem. Phys.*, 2019, **150**, 244508.

38 S. V. Savenko and M. Dijkstra, *J. Chem. Phys.*, 2006, **124**, 234902.

39 A. G. Cherstvy, *J. Phys. Chem. B*, 2008, **112**, 12585–12595.

40 A. Patti and M. Dijkstra, *Phys. Rev. Lett.*, 2009, **102**, 128301.

41 J. A. Wood, Y. Liu and A. Widmer-Cooper, *J. Chem. Phys.*, 2021, **154**, 244505.

42 S. Plimpton, *J. Comput. Phys.*, 1995, **117**, 1–19.

43 G. Torrie and J. Valleau, *J. Comput. Phys.*, 1977, **23**, 187–199.

44 G. Fiorin, M. L. Klein and J. Hénin, *Mol. Phys.*, 2013, **111**, 3345–3362.

45 A. Grossfield, Wham: the weighted histogram analysis method, https://membrane.urmc.rochester.edu/wordpress/?page_id=126, Version 2.0.9.1.

46 V. Ramasubramani, B. D. Dice, E. S. Harper, M. P. Spellings, J. A. Anderson and S. C. Glotzer, *Comput. Phys. Commun.*, 2020, **254**, 107275.

47 E. Frezza, A. Ferrarini, H. Bindu Kolli, A. Giacometti and G. Cinacchi, *Phys. Chem. Chem. Phys.*, 2014, **16**, 16225–16232.

48 S. Belli, S. Dussi, M. Dijkstra and R. van Roij, *Phys. Rev. E: Stat., Nonlinear, Soft Matter Phys.*, 2014, **90**, 020503(R).

49 G. Cinacchi, A. Ferrarini, A. Giacometti and H. B. Kolli, *J. Chem. Phys.*, 2017, **147**, 224903.

50 P. G. Bolhuis, A. Stroobants, D. Frenkel and H. N. W. Lekkerkerker, *J. Chem. Phys.*, 1997, **107**, 1551–1564.

51 N. Chaturvedi and R. D. Kamien, *Proc. R. Soc. A*, 2020, **476**, 20190824.

52 R. D. Kamien and T. Machon, *Proc. Natl. Acad. Sci. U. S. A.*, 2020, **117**, 24102–24109.

53 J. M. Miller, D. Hall, J. Robaszewski, P. Sharma, M. F. Hagan, G. M. Grason and Z. Dogic, *Sci. Adv.*, 2020, **6**, eaba2331.

54 Y. Zhu, J. He, C. Shang, X. Miao, J. Huang, Z. Liu, H. Chen and Y. Han, *J. Am. Chem. Soc.*, 2014, **136**, 12746–12752.

55 W. Feng, J.-Y. Kim, X. Wang, H. A. Calcaterra, Z. Qu, L. Meshi and N. A. Kotov, *Sci. Adv.*, 2017, **3**, e1601159.

56 X. Tao, H. Li, B. Yu, X. Wu, Y. Lu, Y. Wang and H. Chen, *Nanoscale*, 2019, **11**, 19729–19735.

57 H. H. Wensink and C. Ferreiro-Córdova, *Soft Matter*, 2017, **13**, 3885–3893.

58 M. M. C. Tortora, G. Mishra, D. Prešern and J. P. K. Doye, *Sci. Adv.*, 2020, **6**, eaaw8331.